

<sub>1</sub> Determining multi-scale controls on river  
<sub>2</sub> temperature: a time series approach

<sub>3</sub> Michael Vlah and Gordon Holtgrieve

<sub>4</sub> April 19, 2017

## 5 Abstract

6 Temperature is among the most important determinants of riverine biodiversity  
7 and health. It is therefore a primary freshwater management concern, par-  
8 ticularly where temperature-sensitive fish are of high ecological, recreational,  
9 and commercial value. River temperature in the Puget Sound watershed of the  
10 Northwestern U.S.A. is affected by a great diversity of drivers at multiple spatial  
11 and temporal scales, but little is known of their interactions. We used dynamic  
12 factor analysis, a multivariate time-series technique for dimension reduction,  
13 to examine relationships among these drivers, synthesizing long-term climate  
14 and fine-scale land cover data. We found that primarily rain-fed rivers undergo  
15 large seasonal temperature fluctuations, which closely track air temperature,  
16 while snow-fed rivers tend to be more weakly, and in some cases inversely, cou-  
17 pled with air trends. However, variation in coupling among snow-fed rivers is  
18 high, and disproportionately influenced by artificial reservoirs, which appear to  
19 augment the decoupling effect of melting snow and glacial ice in summer. Still,  
20 our results suggest snow-influenced rivers stand to see the largest changes in  
21 temperature regime under projected climate scenarios.

## 22 Introduction

23 The ecological condition of a stream or river, the life it supports, and the goods  
24 and services it provides, are influenced by the timing and magnitude of seasonal  
25 changes in water temperature. Temperature is a chief consideration in the man-  
26 agement of fisheries, as it affects species distribution (Boisneau et al., 2008),  
27 growth and reproduction (McCullough, 1999), and migration timing (Boscarino  
28 et al., 2007). In particular, In the Puget Sound watershed of the American  
29 Pacific Northwest, several salmonid species spawn, migrate, and emerge only  
30 within the bounds of a few degrees Celsius, and thrive under even greater tem-  
31 perature constraints (Carter, 2005). As a result, the success of commercial and  
32 recreational fisheries that depend on the region’s riverine habitat rests on many  
33 precarious factors.

34 River networks, being fractal in structure, are naturally governed by envi-  
35 ronmental processes at multiple scales. Seasonal variation in water temperature  
36 in rivers of the Pacific Northwest is a function of the surrounding air, as well as  
37 precipitation and snowmelt (Eldridge, 1967). These drivers may in turn be me-  
38 diated or supplemented by several aspects of watershed morphology at smaller  
39 scales, including slope, elevation, and geology (Poole and Berman, 2001; Lisi  
40 et al., 2013). Taken together, this hierarchical system complicates fishery man-  
41 agement, as the temperature regime of one river may be the direct product of  
42 climate, while that of another may depend more on within-watershed conditions.

43 Adding to this picture, flow regimes across rivers of the Puget Sound wa-  
44 tershed vary with latitude and elevation (Reidy Liermann et al., 2012; Mauger  
45 et al., 2015), and can be classified broadly into three categories by flow source  
46 and hydrograph shape. Rain-dominated (RD) rivers receive little or no input  
47 from snowmelt, and thus peak in discharge ( $Q$ ) during the rainy season, usu-  
48 ally between October and February. Snow-dominated (SD) rivers instead see  
49 peak flow during spring snowmelt, often in April, May, or June. Between these  
50 extremes lies a third class of rain-and-snow-driven (RS) rivers, which have ap-  
51 preciable peaks at both times.

52 Effective management plans must therefore integrate a diversity of factors  
53 across space and time in order to determine which rivers and watersheds are  
54 likely to see consequential changes under projected climate and land use sce-  
55 narios for the Pacific Northwest (Mote and Salathe, 2010; Radeloff et al., 2012).  
56 However, the understanding required to do so is limited by knowledge of rela-  
57 tionships among temperature drivers at scale.

58 We sought to identify rivers in the Puget Sound region whose temperatures  
59 fluctuate closely with regional trends in air temperature, precipitation, and  
60 snowmelt, and those that depart from regional patterns. Our second aim was  
61 to identify watershed features that correlate with such departures, and thus  
62 provide a nuanced basis for predicting impacts of water temperature on aquatic  
63 biodiversity and fishery health. We hypothesized that water temperature ( $T_{\text{water}}$ )  
64 would track air temperature  $T_{\text{air}}$  most closely in RD rivers (Ward, 1985; Garner  
65 et al., 2014). We expected deviations from this relationship to correlate best  
66 with cold-water influx from snow and ice melt (Lisi et al., 2015) and with factors

67 affecting heat capacity of water, including  $Q$  (volume over time) and watershed  
68 slope (which relates to turbulence, surface area, and mixing; van Vliet et al.  
69 2013).

## 70 **Methods**

### 71 **Water and climate data**

72 We investigated climate and landscape controls on  $T_{\text{water}}$  and  $Q$ , as separate  
73 response variables, from 1978 to 2015. Monthly time series of water tempera-  
74 ture were obtained for 24 river sites via the Washington Department of Ecol-  
75 ogy’s River and Stream Water Quality Monitoring program (Von Prause, 2017).  
76 These sites represent 19 nonnested watersheds across 9 counties, and range from  
77 4 to 775 m in elevation. For at least one site at each river, monthly  $Q$  time se-  
78 ries were also available, either from the same location as one of the temperature  
79 monitoring sites, or from within 30 km on the same major reach.  $Q$  data were  
80 aggregated by monthly mean from the USGS National Water Information Sys-  
81 tem database (USGS, 2017).

82

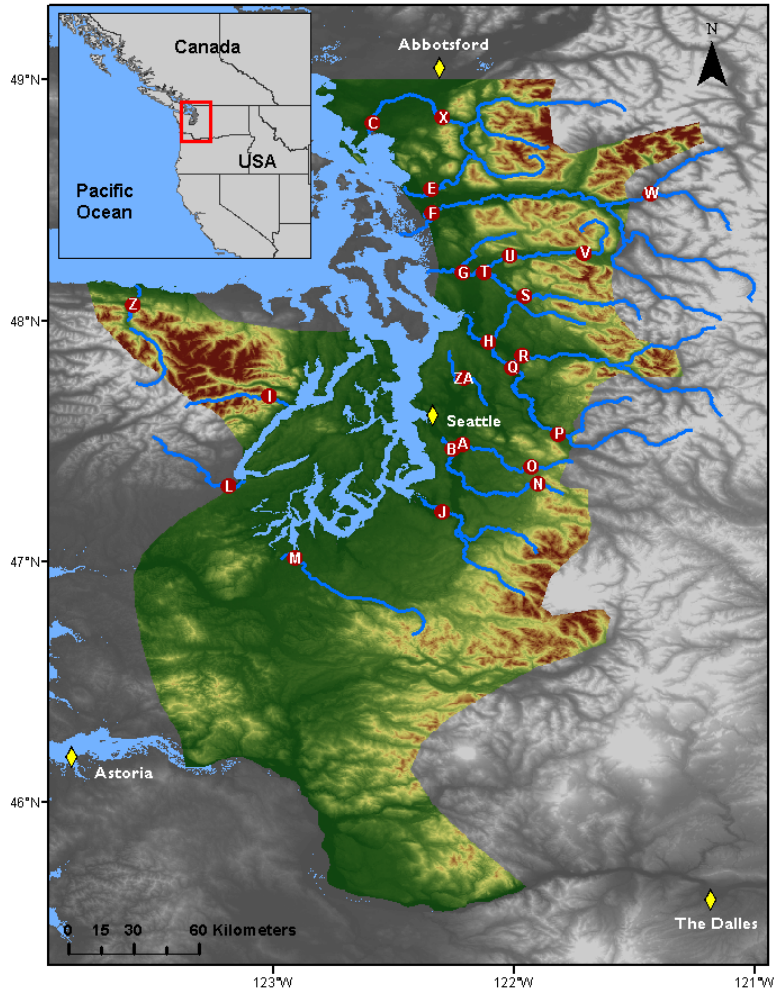


**Figure 1** Site locations (red points) in relation to combined Washington State Climate Divisions 3 and 4 (colored topography), the region across which climate data were aggregated. See Appendix C for site information.

Potential climatic predictors of  $T_{\text{water}}$  and  $Q$  included mean and max  $T_{\text{air}}$  ( $^{\circ}\text{C}$ ), total precipitation (cm), snowmelt (cm), and hydrological drought (Palmer Hydrological Drought Index), averaged by month across the response variable time series. All but snowmelt were available through the U.S. Climate Divisional Dataset, developed by the National Centers for Environmental Informa-

tion (NCEI; NOAA 2017). We acquired climatic predictor data grouped by Washington State climate division, and all but two of our sites fell within divisions 3 (Puget Sound Lowland) and 4 (East Olympic/Cascade Foothills; see Fig. 1). We therefore aggregated these data by monthly mean across the two regions (after verifying their post-standardization similarity), resulting in a single dataset of four climatic predictor variables. A snowmelt time series was then added to this dataset, using monthly mean records from six SNOTEL sites (Bumping Ridge, Elbow Lake, Mount Crag, Park Creek Ridge, Stevens Pass, White Pass) listed by the USDA’s Natural Resources Conservation Service; USDA 2017. We calculated monthly snowmelt for each site as the absolute value of negative differences in cumulative snow water equivalent from each month to the next. The snowmelt time series was assigned zeros for any positive differences (accumulations).

## Time series analysis

Response time series ( $T_{\text{water}}$  and  $Q$ ) were modeled using dynamic factor analysis (DFA; Zuur et al. 2003b), a multivariate technique that can be thought of as an analog to principal component analysis in the time domain. In DFA, response time series are fit with a linear combination of shared, random-walk trends (usually many fewer than the total number of response series), predictors (which can have unique effects on each response series), and random error. We chose DFA over a traditional multivariate state space approach for two reasons. First, it provides advantages in computational efficiency, as a small number of shared trends often adequately capture variation across dozens of responses, and at much lower parameter cost (Zuur et al., 2003a). Second, in terms of identifying what drives the shared trends, having fewer of them allows for greater inferential parsimony. Being a multivariate technique, DFA also provides an advantage over univariate alternatives in that covariance structure among responses can be specified and compared. All models were fit using maximum likelihood estimation by automatic differentiation, with Template Model Builder software (Kristensen et al., 2015), which we called using package TMB in R (R Core Team, 2017; Kristensen et al., 2016).

DFA takes the following form:

$$\mathbf{x}_t = \mathbf{x}_{t-1} + \mathbf{w}_t, \text{ where } \mathbf{w}_t \sim \text{MVN}(0, \mathbf{Q}) \quad (1)$$

$$\mathbf{y}_t = \mathbf{Z}\mathbf{x}_t + \mathbf{D}\mathbf{d}_t + \mathbf{v}_t, \text{ where } \mathbf{v}_t \sim \text{MVN}(0, \mathbf{R}) \quad (2)$$

$$\mathbf{x}_0 \sim \text{MVN}(0, \mathbf{\Lambda}) \quad (3)$$

At time step  $t$ , the  $m \times 1$  vector of shared trends ( $\mathbf{x}$ ) is a function of  $\mathbf{x}$  in the previous step, plus normal error ( $\mathbf{w}$ ;  $m \times 1$ ; Eq. 1). This is the definition of a random walk. The  $n \times 1$  response vector ( $\mathbf{y}$ ) at time  $t$  is a function of the shared trends and their factor loadings ( $\mathbf{Z}$ ;  $n \times m$ ), covariates ( $\mathbf{d}$ ;  $q \times 1$ ) and their river-specific effects ( $\mathbf{D}$ ;  $n \times q$ ), and a second normal error term ( $\mathbf{v}$ ;  $n \times 1$ ; Eq. 2).  $\mathbf{R}$  and  $\mathbf{Q}$  are variance-covariance matrices of order  $m$ , and  $\mathbf{Q}$  is

set to identity for model identifiability (Harvey, 1990). The initial state of the shared trend vector ( $\mathbf{x}_0$ ) is multivariate-normally distributed with a mean of zero and a diagonal variance-covariance matrix with large variance (e.g. 5; Eq. 3). Response and predictor data were standardized to facilitate comparison of effect sizes and avoid error inflation.

Because we were interested in isolating the effects of climatic predictors on  $T_{\text{water}}$  and  $Q$ , we used a fixed factor to account for recurring seasonal variation not related to the predictors, with one factor level for each month. This factor was incorporated into the covariate matrix ( $\mathbf{d}$ ). Thus, the coefficient in  $\mathbf{D}$  relating, say, precipitation (predictor) and  $T_{\text{water}}$  (response), represents the effect size of the former on the latter. In other words, it is the change in water temperature accompanying a unit change in precipitation across the whole time series. We call this relationship “coupling.” We were also interested in coupling by month for  $T_{\text{air}}$ , which required that it be arranged as twelve separate, monthly time series. Concretely,

$$\mathbf{d} = \begin{matrix} & \text{Jan}_{1978} & \text{Feb}_{1978} & \text{Mar}_{1978} & \cdots & \text{Dec}_{2015} \\ \begin{matrix} 1 \\ 2 \\ 3 \\ \vdots \\ 12 \\ 13 \\ 14 \\ 15 \\ 16 \\ 17 \\ \vdots \\ 26 \end{matrix} & \left( \begin{array}{ccccc} 1 & 0 & 0 & \cdots & 0 \\ 0 & 1 & 0 & \cdots & 0 \\ 0 & 0 & 1 & \cdots & 0 \\ \vdots & \vdots & \vdots & \ddots & \vdots \\ 0 & 0 & 0 & \cdots & 1 \\ \textit{precip}_1 & \textit{precip}_2 & \textit{precip}_3 & \cdots & \textit{precip}_{456} \\ \textit{snowmelt}_1 & \textit{snowmelt}_2 & \textit{snowmelt}_3 & \cdots & \textit{snowmelt}_{456} \\ \textit{air}_1 & 0 & 0 & \cdots & 0 \\ 0 & \textit{air}_2 & 0 & \cdots & 0 \\ 0 & 0 & \textit{air}_3 & \cdots & 0 \\ \vdots & \vdots & \vdots & \ddots & \vdots \\ 0 & 0 & 0 & \cdots & \textit{air}_{456} \end{array} \right) \end{matrix}$$

is the covariate matrix structure necessary to account for seasonal variation of unknown origin (rows 1-12), and the effects of precipitation (row 13) and snowmelt (row 14), while also yielding the effect of  $T_{\text{air}}$  by month (rows 15-26) on the response ( $\mathbf{y}$ ; Eq. 2). This is the covariate structure of the  $T_{\text{water}}$  model we used for subsequent analyses, not including those described in Figure 5d-e, and Appendix B. The same form was used for the  $Q$  model.

Additional, non-seasonal variation due to unknown factors manifests in the shared trends, and a portion of any residual variation is absorbed by error matrix  $\mathbf{v}$ . We fit models using four unique error structures ( $\mathbf{R}$ ), to allow for multiple suites of unknown drivers affecting rivers. We included shared variance with zero covariance, individual variance with zero covariance, shared variance with shared covariance, and individual variance with individual covariance. Details on these structures and their implications can be found in (Holmes et al., 2012). The best models for  $T_{\text{water}}$  and  $Q$  were determined via AIC. However, negligible likelihood

improvements can be inflated when multiplied by thousands of data points, undermining common rules of thumb for admitting additional parameters under AIC (Burnham and Anderson, 2003). Thus, we had reason to doubt that the “most parsimonious” model according to AIC alone was any better than a much simpler alternative. To manage this, we required that each additional trend, covariate, or seasonal structure improve the median coefficient of determination ( $R^2$ ) by at least 1% in order to justify accepting its attendant complexity.

## Landscape predictors and post-hoc regression

For post-hoc analyses, monitoring sites were separated into three classes based on relative areal coverage of perennial ice and/snow (hereinafter “% glaciation”) and mean elevation across their watersheds. The three classes are loosely based on the classification scheme and language of the Climate Impacts Group at the University of Washington (Mauger et al., 2015), and are here delineated according to Table 1.

**Table 1** Watershed classification scheme

Classification	Abb.	Glaciation (%)	Mean elev. (m)
Rain-dominated	RD	$< 0.7$	$< 600$
Rain-and-snow	RS	$< 0.7$	$\geq 600$
Snow-dominated	SD	$\geq 0.7$	-

After model selection, climatic predictor effect sizes ( $\mathbf{D}$ ; Eq. 2) for each river were back-transformed to their original scales and regressed against landscape predictors in order to identify possible watershed-scale controls on coupling. To achieve this, we amassed an additional dataset of landscape features (Appendix C). These were collected individually for each of the watersheds corresponding to our 24 river sites, using the EPA’s StreamCat (stream-catchment) data library (Hill et al., 2016) and the National Hydrography Dataset (NHDPlusV2; McKay et al. 2012). Each site was mapped to an individual river reach, defined as a segment bounded on each end by a stream or river source, confluence, or mouth. The region contributing flow to this reach (its watershed) was then fetched, along with selected areal data, from the NHDPlusV2 database. Landscape attributes used as predictors were aggregated by watershed mean where applicable, and include elevation (m), total area ( $\text{km}^2$ ), soil permeability ( $\text{cm hr}^{-1}$ ), water table depth (cm), bedrock depth (cm), Base Flow Index (BFI; %), runoff ( $\text{mm mo}^{-1}$ ), percent perennial ice and snow coverage (National Land Cover Database [NLDC] 2006 and 2011 average), riparian population density (people  $\text{km}^{-2}$  within 100m of streams; 2010 census), riparian road density ( $\text{km km}^{-2}$ ; 2010 census), and percent riparian urban land (NLCD 2011). Monitoring site elevation (m) and presence of upstream dams (as full/partial/no damming of upstream mainstem and major tributaries) were also included. Finally, we calculated area above 1000 m (as % watershed area), mean slope (% rise), and mean aspect (degree from true north) by delineating and summarizing watersheds from a digital elevation model in ArcMap v. 10.4 (ArcMap, 2016).



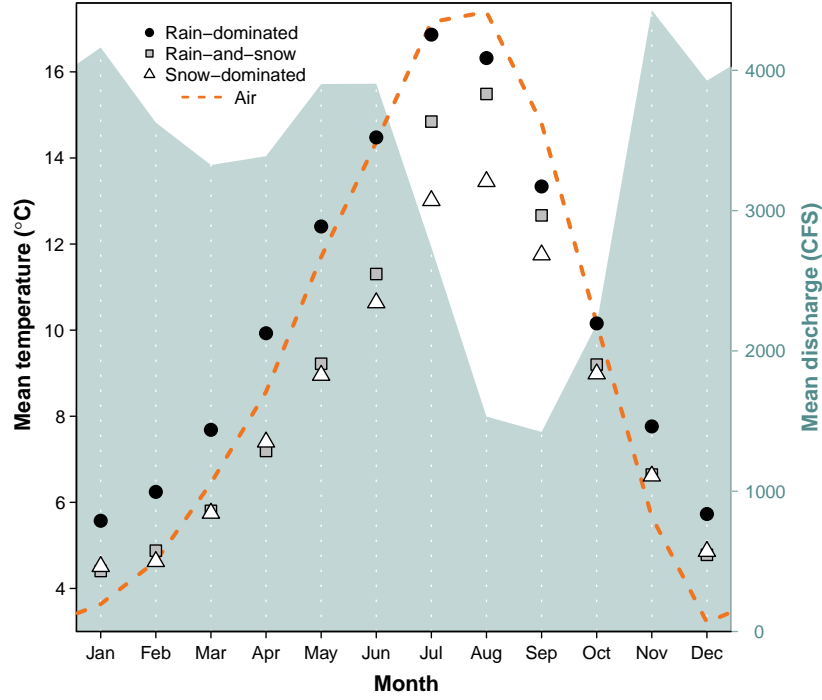
200 An additional set of post-hoc regressions was performed using factor load-  
 201 ings on shared trends ( $\mathbf{Z}$ ; Eq.2) as dependent variables, with landscape predic-  
 202 tors again as independent variables. Loadings represent the degree to which  
 203 each river’s temperature fluctuates with the anonymous force driving the corre-  
 204 sponding shared trend. A landscape feature that varies in proportion to these  
 205 loadings is therefore likely to be a mediator of the anonymous force, if not the  
 206 force itself. To facilitate inference by way of the shared trends, we made three  
 207 simplifications to the model. We removed the monthly factor and the snowmelt  
 208 predictor from the covariate matrix ( $\mathbf{d}$ , rows 1-12 and 14), so that the trends  
 209 would be free to express seasonal and elevational variation. Then, we limited  
 210 the number of trends to between one and three, to avoid “trend specialization.”  
 211 in other words, we optimized the trends for flexibility while concentrating their  
 212 explanatory power. Additionally, we ordinated the landscape predictors with  
 213 principal coordinates analysis (PCoA), as a way to conceptually “group” them  
 214 by correlation. Data constrained to irregular, restricted ranges were scaled to  
 215 [0-1] and arcsine-square-root transformed, along with all proportional data (The  
 216 logit transform was avoided to prevent generation of infinite values.). All con-  
 217 tinuous data were then centered and scaled to unit variance before PCoA was  
 218 performed. We used the Gower dissimilarity coefficient (Gower’s distance) to  
 219 account for association among both continuous and nominal variables (Gower,  
 220 1966).

## 221 Results

222 Mean monthly temperature trends for the three river classes, aggregated across  
 223 all 38 years of data, deviated by a minimum of 1.0°C in December, and a  
 224 maximum of 3.9°C in July (Fig. 2). SD rivers remained approximately two  
 225 degrees colder than their RS counterparts through mid-late summer, and 3-  
 226 4 degrees colder than RD throughout spring and summer. RD rivers were  
 227 consistently warmest throughout the year. In January, RS reached a minimum of  
 228 4.4°C, and did not significantly differ from SD (Student’s  $t$ :  $p < 0.01$ ,  $F = 11.9$ ).  
 229 RD only attained a minimum of 5.6°C. RS reached a peak summer temperature  
 230 of 16.9°C in July, while RS and SD followed in August with peak temperatures  
 231 of 15.5 and 13.5°C, respectively.

232 Meanwhile, the amplitude of  $T_{\text{air}}$  oscillation exceeded that of any river class,  
 233 dipping below  $T_{\text{water}}$  in autumn to a minimum of 3.2°C in December, and  
 234 rising above RS and SD in March to an August maximum of 17.4°C.  $T_{\text{air}}$  did  
 235 not overtake RD  $T_{\text{water}}$  until August, by which time the latter had begun to  
 236 decline.

237



238

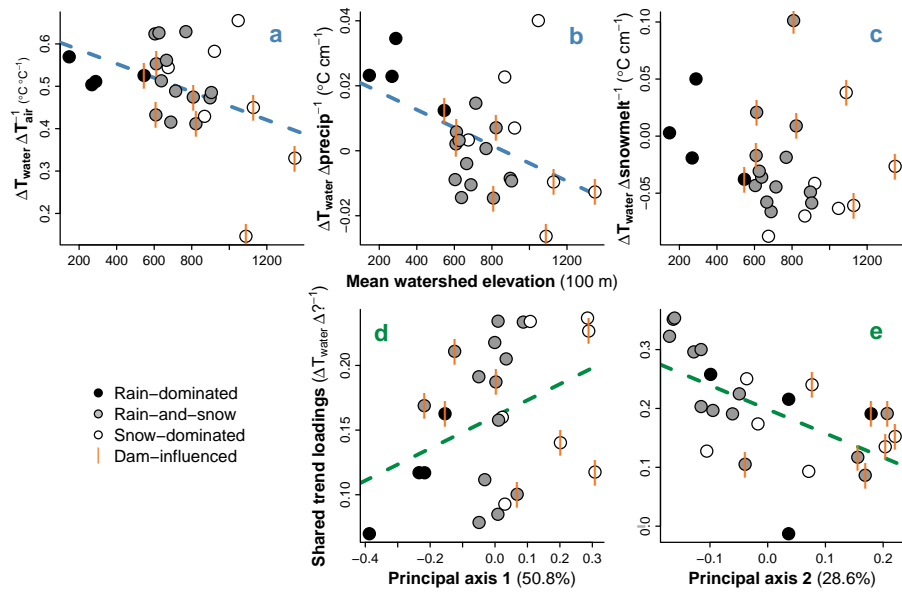
239 **Figure 2** Monthly mean  $T_{\text{water}}$  by river class, and  $T_{\text{air}}$  and  $Q$  across classes,  
 240 from 1978 to 2015. All depicted series represent discrete data.

241

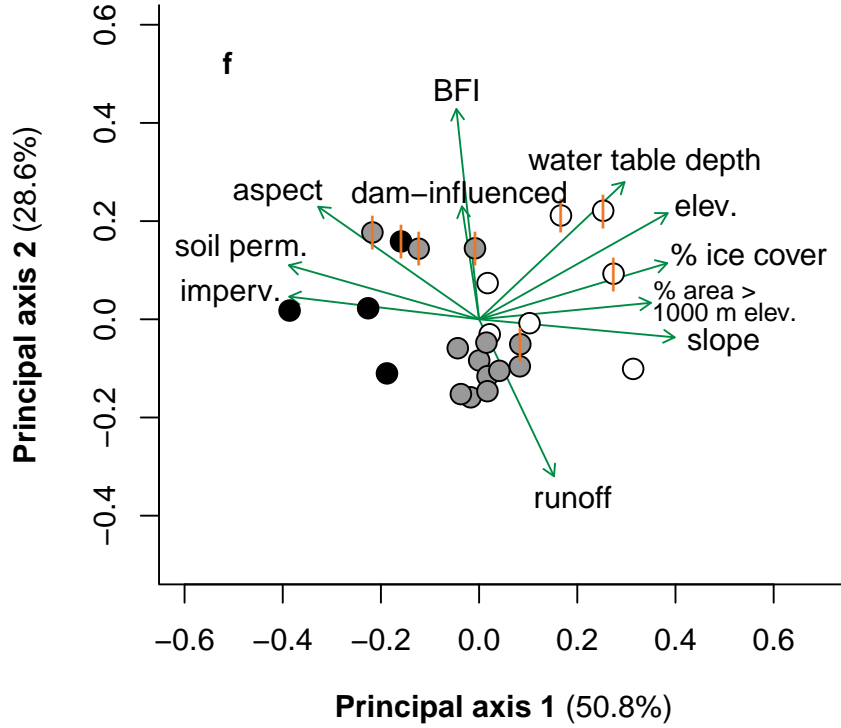
242 The combined hydrograph of all rivers revealed two primary peaks, one be-  
 243 ginning in late spring and the other extending from late autumn to early winter,  
 244 with a prominent trough in late summer. Spring peak  $Q$  coincided noticeably  
 245 with a separation in water temperature between SD and RS, while the sum-  
 246 mer trough coincided with separation of RD and  $T_{\text{air}}$ . On average, November  
 247 marked both the autumn peak in  $Q$  and the point at which  $T_{\text{air}}$  fell below  
 248  $T_{\text{water}}$ .

249 There was also an apparent divergence in slope between RD and all snow-  
 250 influenced rivers, beginning in early spring and culminating in June. Between  
 251 June and July, RS and SD saw a large jump in temperature, which coincided  
 252 with the decline in snowmelt.

253



254



255

256 **Figure 3** (a-c) Relationships between watershed elevation and climatic effects  
 257 on  $T_{\text{water}}$ , obtained from full model fit. (d-e) Relationships between watershed  
 258 features and factor loadings on shared trends, from constrained model fit. Re-  
 259 gression lines indicate slopes significant at  $\alpha = 0.1$ . (f) Ordination of landscape  
 260 predictors by principal coordinates analysis. Length and direction of arrows are  
 261 proportional to loading of landscape predictors onto each principal axis of their  
 262 variation.

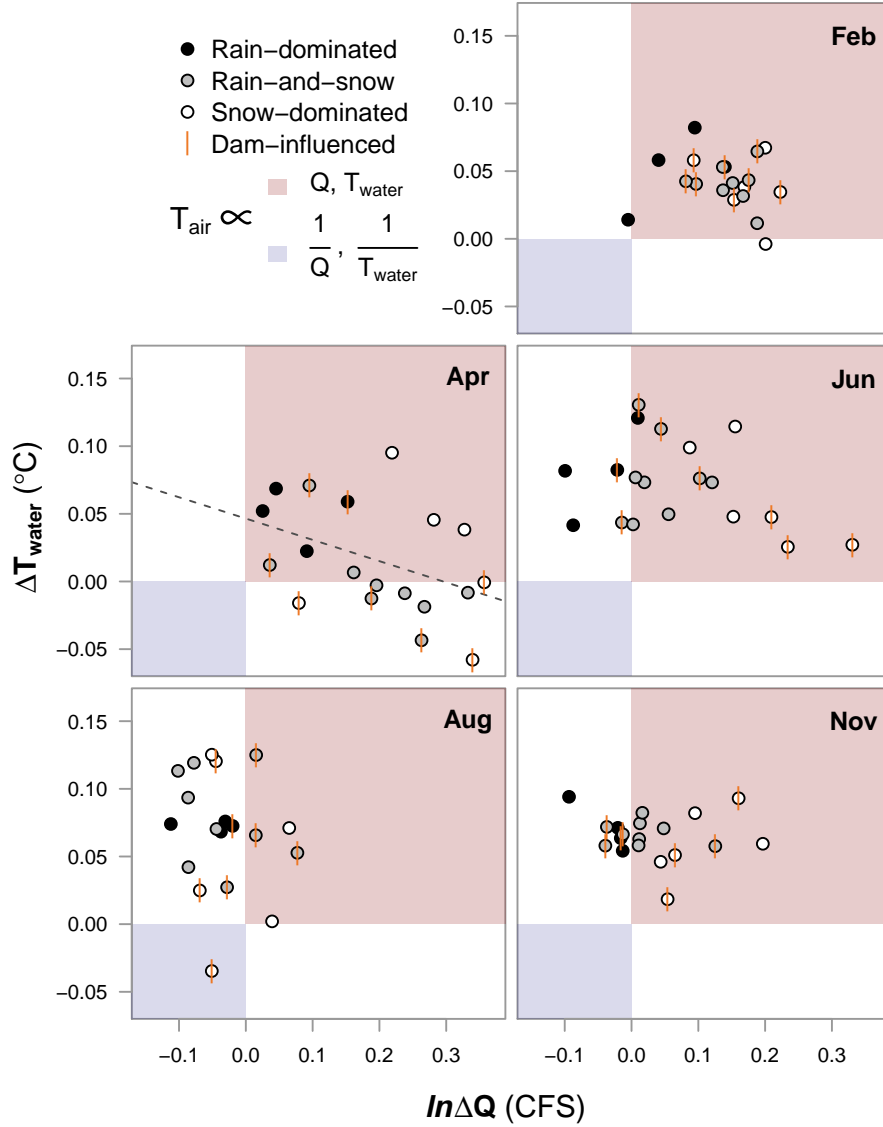
263

264 DFA results, aggregated across months and years for each site, revealed a  
 265 trend toward reduced  $T_{\text{air}} \rightarrow T_{\text{water}}$  coupling with increasing watershed el-  
 266 evation ( $p = 0.04$ ,  $\text{mult.}R^2 = 0.18$ ; Fig. 3a). On average, a  $1^\circ\text{C}$  change in  
 267  $T_{\text{air}}$  corresponded to a  $0.53 \pm 0.03^\circ\text{C}$  change in  $T_{\text{water}}$  at RD, a  $0.51 \pm 0.08^\circ\text{C}$   
 268 change at RS, and a  $0.45 \pm 0.17^\circ\text{C}$  change at SD sites. A similar trend was  
 269 observed with respect to  $\text{precip} \rightarrow T_{\text{water}}$  coupling ( $p = 0.03$ ,  $\text{mult.}R^2 = 0.21$ ;  
 270 Fig. 3b), where a monthly change in total precipitation of 1 cm corresponded

271 to a  $0.02 \pm 0.009^{\circ}\text{C}$  change in  $T_{\text{water}}$  for RD,  $-0.003 \pm 0.009^{\circ}\text{C}$  for RS, and  
 272  $0.004 \pm 0.02^{\circ}\text{C}$  for SD. There was no evidence of coupling overall between  
 273 snowmelt and  $T_{\text{water}}$  (Fig. 3c), but this predictor was included in the most  
 274 parsimonious DFA model selected via AIC and  $R^2$  (See Appendix A.). The  
 275 strongest examples of  $T_{\text{air}} \rightarrow T_{\text{water}}$  and  $\text{precip} \rightarrow T_{\text{water}}$  coupling were ob-  
 276 served in the Duckabush River, while the weakest examples are from the Elwha  
 277 River. Both rivers drain glaciers of the Olympic Mountain Range, and both are  
 278 SD. Among SD rivers, those influenced by dams appear to couple less strongly  
 279 with  $T_{\text{air}}$  and  $\text{precip}$ , but more so with snowmelt.

280 Factor loadings from a constrained, two-trend model each correlated with  
 281 one of the two dominant, principal axes of variation across landscape predictors,  
 282 determined by PCoA (Fig. 3f). The first principal axis was driven by mean  
 283 watershed slope, snow (% area  $> 1000$  m) and ice, soil permeability, and other  
 284 features that vary along elevational gradients, as well as mean elevation itself.  
 285 Watershed's scores along this axis correlated with loadings from one trend, with  
 286 marginal significance ( $p = 0.07$ ,  $\text{mult.}R^2 = 0.14$ ; Fig. 3d). The second principal  
 287 axis was driven by runoff, base flow, and upstream dams, and correlated with  
 288 the other trend's loadings ( $p < 0.01$ ,  $\text{mult.}R^2 = 0.35$ ; Fig. 3e). Combined,  
 289 the first two principal axes accounted for 79.4% of variation across landscape  
 290 predictors.

291



292

293 **Figure 4** Relationship between  $T_{\text{air}} \rightarrow T_{\text{water}}$  and  $T_{\text{air}} \rightarrow Q$ . Both axes are  
 294 expressed per  $1^{\circ}\text{C}$  change in  $T_{\text{air}}$ . The red quadrant designates proportionality  
 295 between all three variables, the blue inverse proportionality between each re-  
 296 sponse and  $T_{\text{air}}$ . Regression lines indicate slopes significant at  $\alpha = 0.05$ .

297

298 To examine possible sub-season interactions between  $T_{\text{air}}$ ,  $T_{\text{water}}$  and  $Q$ , we  
 299 performed an additional DFA with  $Q$  as the response. In both models,  $T_{\text{air}}$

was allowed to have unique monthly effects. These effects, taken together, can be conceptualized in relation to the four quadrants of the Cartesian coordinate system (increasing clockwise from upper right; Fig. 4).

In mid-winter (exemplified by February), all river classes primarily occupy the first quadrant, signifying  $T_{\text{air}} \propto T_{\text{water}}$  and  $T_{\text{air}} \propto Q$ , where  $\propto$  denotes proportionality. RD shows the weakest  $Q$  response. By spring, many RS and SD sites develop an inverse relationship between  $T_{\text{air}}$  and  $T_{\text{water}}$ , denoted  $T_{\text{air}} \propto \frac{1}{T_{\text{water}}}$ , while RD sites change little from their winter state. June and August see a procession of most sites into the near fourth quadrant, with SD trailing. This signifies  $T_{\text{air}} \propto \frac{1}{Q}$ , though  $T_{\text{air}} \propto T_{\text{water}}$ . One stark exception is again the Elwha river, which occupies quadrant three. By autumn, RS and SD have begun progress back toward their winter states, led by SD. RD, meanwhile, remain essentially unmoved from summer.

Rivers influenced by dams do not appear to deviate appreciably from the rest in February, August, or November. However, SD rivers in April divide across the x-axis according to whether they are dammed. Those with dams exhibit  $T_{\text{air}} \propto \frac{1}{T_{\text{water}}}$ , while  $T_{\text{air}} \propto T_{\text{water}}$  for those without. Similarly, in June, dammed SD rivers display stronger coupling between  $T_{\text{air}}$  and  $Q$  than those without dams.

## Discussion

The effects of climate on  $T_{\text{water}}$ , inferred through dynamic factor analysis, suggest that nearly all rivers included in our dataset were influenced strongly by air temperature, precipitation, and/or snowmelt across 38 years of monthly data (Fig. 3a-c). At most monitoring sites,  $T_{\text{water}}$  closely tracked changes in  $T_{\text{air}}$ , on average responding to increases and decreases with proportional movements of up to 66% magnitude. However, some rivers only weakly tracked  $T_{\text{air}}$ , and patterns in the intensity of this coupling relate primarily to changing landscape features along an elevational gradient (Fig. 3f). Glaciation and yearly snow burden are prominent among these, and for reasons of ecological and hydrological implication, the primary focus of the following discussion, along with the interacting role of dams.

Before any analysis, a “buffering” effect (the inverse of coupling) of ice on river temperature can be seen in the yearly patterns of  $T_{\text{water}}$  relative to  $T_{\text{air}}$  (Fig. 2). The aggregate hydrograph peaks due to snowmelt from April to June, at the same time that the trajectories of RS and SD (snow-influenced rivers) start to drop off relative to RD. After snowmelt begins to subside, RS and SD recover with a noticeable jump. For rivers that receive glacial runoff (SD), this buffering effect appears to remain into the summer months, guarding them from temperature rise when RS rivers instead approach the temperature of RD (Fig. 4). In an extreme case, the Elwha River was actually cooler in August during those years in which air temperature was higher, probably due to increased runoff from Carrie and Eel glaciers. The buffering effect of ice on river temperature is therefore two-fold, acting first on all snowmelt-influenced

343 rivers through a cold-water pulse in spring, and then on a subset of those rivers  
 344 throughout summer and autumn, by way of glacial runoff. For RD rivers, which  
 345 receive little to no input from ice, summer temperature is entirely dictated by  
 346 that of the surrounding air, and any rain falling through it.

347 Temperature buffering by snow and ice appears to be enhanced by the action  
 348 of artificial impoundments. Eight sites on five rivers included in this study are  
 349 (or were until 2014, in the case of the Elwha River) interrupted by dams or  
 350 embankments that release stored water from the bases of their reservoirs. At 33  
 351 m, even the shallowest of these reservoirs is deep enough to stratify in summer,  
 352 meaning released water would be delivered from the cold hypolimnion (Olden  
 353 and Naiman, 2010). This certainly would have affected temperature readings  
 354 for the Green, Elwha, Cedar and upper Skagit River sites, whose mainstems are  
 355 or were dammed upstream of the sample location. The impact of damming on  
 356 temperature readings at the Skokomish and the lower Skagit River sites should  
 357 be lesser, as major, unobstructed river forks intercede between sample location  
 358 and dam, resetting or partially resetting natural conditions (Stanford and Ward,  
 359 2001). These sites are RS and SD, respectively, and both fall almost exactly  
 360 on the regression line in Figure 4a. The upper Skagit site therefore occupies  
 361 a middling space of  $T_{air} \rightarrow T_{water}$  coupling between “fully” obstructed and  
 362 unobstructed SD sites.

363 As for the unobstructed SD sites, they appear to oppose the trend exem-  
 364 plified overall. In particular, the Duckabush and Puyallup Rivers (upper white  
 365 circles in Figs 3a, 3b, and 4-Apr.) noticeably break suit with the other SD sites  
 366 in terms of  $T_{air} \rightarrow T_{water}$  and precip.  $\rightarrow T_{water}$ , showing stronger relationships  
 367 even than many of the RD rivers. Compared to all RS and RD rivers, and many  
 368 SD, these stand out in terms of mean water table depth (Appendix C), suggest-  
 369 ing they receive little influence from groundwater influx, which would otherwise  
 370 serve to decouple  $T_{air}$  and  $T_{water}$ . They also occupy smaller watersheds than  
 371 most of the other SD rivers, which yield lower overall discharge and heat ca-  
 372 pacity, and thus greater susceptibility to temperature change (Caissie, 2006).  
 373 There may be additional factors at work in the SD rivers that account for the  
 374 surprisingly high coupling seen in some unobstructed SD rivers. Another po-  
 375 tential candidate is watershed slope, which increases with elevation and affects  
 376  $T_{water}$  by influencing residence time and evaporative cooling (via turbulence).  
 377 High slope and elevation are also associated with lower-order tributaries, and  
 378 thus lower heat capacity.

379 The role of reservoirs in restructuring natural temperature coupling rela-  
 380 tionships is complex (Webb and Walling, 1997; Gooseff et al., 2005), and here  
 381 confounded with many additional variables. Omitting all obstructed sites from  
 382 Figure 3a, it would appear that no trend exists, yet we believe such omission  
 383 is unwarranted. If the presence of reservoirs negated the influence of other fac-  
 384 tors, there would be no separation between obstructed sites of different river  
 385 classes. Furthermore, though cold, hypolimnetic outflow should be expected  
 386 to buffer  $T_{water}$  in summer, it alone cannot explain an *inverse* relationship be-  
 387 tween  $T_{air}$  and  $T_{water}$ . Instead, reservoirs may serve to enhance the decoupling  
 388 of  $T_{air} \rightarrow T_{water}$  and precip.  $\rightarrow T_{water}$  brought on by snowmelt and glacial



runoff, by selectively withholding warm water in their epilimnia and admitting cold water through their hypolimnia. Evidence for this phenomenon can be seen in the coupling of snowmelt and  $T_{\text{water}}$ , which is generally greater in RS and SD sites downstream of obstructions (Fig. 3c). The Elwha River, which was cleared of its two dams between 2011 and 2014, will provide an excellent opportunity to compare each form of coupling with and without reservoirs, using the same dataset, once enough time has passed for signals to overcome inter-annual variability.

Though higher-elevation watersheds will always produce colder water, independent of the influence of ice and snow, it can be expected that RS and SD rivers will grow more similar to RD as regional temperatures warm and glaciers decline. That is to say, formerly reliably cold-water rivers and associated habitats may see increases in both summer and winter average temperatures, as well as higher variability from year to year. The Elwha in particular may slip from its current state of high resistance to seasonal climatic changes. We tested for changes in mean and variance of  $T_{\text{air}} \rightarrow T_{\text{water}}$  and  $T_{\text{air}} \rightarrow Q$  coupling between 1978 and 2015, but did not detect any regular patterns (Appendix B).

In addition to the most parsimonious DFA, we fit a simplified model, designed to focus on what variation in  $T_{\text{water}}$  could be explained by landscape predictors. The two trends of this model represent additional drivers responsible for structuring water temperature across some or all of the 24 sites included in the analysis. While the precise identities of these drivers cannot be obtained with certainty, they can be inferred through their relationships with predictor variables. In this way, we found elevation to be one of the dominant determinants of  $T_{\text{air}} \rightarrow T_{\text{water}}$  and  $\text{precip.} \rightarrow T_{\text{water}}$ , by driving variation in snow- and icemelt, soil permeability, and slope (Fig. 3f). Dams (reservoirs) and BFI (essentially groundwater contribution) were also major components of variation in temperature coupling, along with water table depth. Groundwater, being insulated from the air, maintains relatively constant temperatures throughout the year, particular if it is deep underground.

The relationship between climate and river temperature is further influenced by the interaction of discharge, and the fates of rivers in the Puget Sound watershed can be best understood by examining these factors in combination (Fig. 4). Whether rain-, both-, or snow-dominated, all rivers appear to take on RD characteristics in winter, when the effects of ice lay latent. As a result, warmer winters should on average yield warmer rivers and higher flow (less precipitation bound in ice). The critical differences between river classes play out in spring and summer, and it's during these months that future perturbations due to changing climate may be felt most acutely. For example, warmer Aprils on average produced colder water at 9 out of 15 RS and SD sites. Projected reductions in snowpack for the Pacific Northwest can therefore be expected to fundamentally alter the responses of currently snow-influenced rivers to yearly variation in spring temperature. In the longer term, changes can be expected for rivers that now receive the temperature-buffering effect of glacial runoff. Glaciers continue to decline across North America, with glacial ice across Western Canada projected to decline by 70% from 2005 to 2100 (Clarke et al., 2015).

## Conclusion

Temperature regimes across the rivers of the Puget Sound watershed are structured by a combination of climatic drivers at the regional scale, and geophysical drivers at watershed scales. In the absence of snow and ice, river temperature is closely coupled to that of the surrounding air, while discharge contributions from snowmelt and glacial runoff can dampen or even reverse this coupling in spring and summer, particularly where hypolimnetic-release reservoirs augment downstream cooling. In some cases, icemelt-influenced rivers exhibit stronger positive responses to climate patterns than their rain-driven counterparts. Our results suggest elevational variations in groundwater influx and total discharge may account for these patterns. However, while these factors and artificial reservoirs may influence the degree of coupling between climatic drivers and water temperature, only snow and ice can reverse it. Since 1978, such reversals have been widespread and commonplace, particularly during spring melt. Though we did not detect changes in this effect across historical observations, future reductions in snowpack and glacial mass are projected. Consequently, many rivers that now undergo the mildest seasonal temperature changes may be impacted most strongly.

## 453 Acknowledgements

454 We thank Timothy Cline for the use of his TMB script, and Drs. Mark Scheuerell,  
455 Eric Ward, Eli Holmes, and Adrienne Smits for technical advice. Drs. Daniel  
456 Schindler and Michael Brett provided additional suggestions and guidance.

## 457 References

- 458 ArcMap (2016). Environmental systems research institute (esri). *Redlands, CA:*  
459 *<http://www.esri.com/>.*
- 460 Boisneau, C., Moatar, F., Bodin, M., and Boisneau, P. (2008). *Does global warm-*  
461 *ing impact on migration patterns and recruitment of Allis shad (Alosa alosa*  
462 *L.) young of the year in the Loire River, France?*, pages 179–186. Springer  
463 Netherlands, Dordrecht.
- 464 Boscarino, B. T., Rudstam, L. G., Mata, S., Gal, G., Johannsson, O. E., and  
465 Mills, E. L. (2007). The effects of temperature and predatorprey interactions  
466 on the migration behavior and vertical distribution of mysis relicta. *Limnology*  
467 *and Oceanography*, 52(4):1599–1613.
- 468 Burnham, K. P. and Anderson, D. R. (2003). *Model selection and multimodel*  
469 *inference: a practical information-theoretic approach*. Springer Science &  
470 Business Media.
- 471 Caissie, D. (2006). The thermal regime of rivers: a review. *Freshwater Biology*,  
472 51(8):1389–1406.
- 473 Carter, K. (2005). The effects of temperature on steelhead trout, coho salmon,  
474 and chinook salmon biology and function by life stage. *Implications for the*  
475 *Klamath River total maximum daily loads. California Regional Water Quality*  
476 *Control Board. North Coast Region, Santa Rosa, California.*
- 477 Clarke, G. K., Jarosch, A. H., Anslow, F. S., Radić, V., and Menounos, B.  
478 (2015). Projected deglaciation of western canada in the twenty-first century.  
479 *Nature Geoscience*, 8(5):372–377.
- 480 Eldridge, E. (1967). Water temperature: influences, effects, and control.  
481 Technical report, Federal Water Pollution Control Administration, Portland,  
482 Oreg.(USA). Northwest Region.
- 483 Garner, G., Hannah, D. M., Sadler, J. P., and Orr, H. G. (2014). River temper-  
484 ature regimes of england and wales: spatial patterns, inter-annual variability  
485 and climatic sensitivity. *Hydrological Processes*, 28(22):5583–5598.
- 486 Gooseff, M. N., Strzepek, K., and Chapra, S. C. (2005). Modeling the poten-  
487 tial effects of climate change on water temperature downstream of a shallow  
488 reservoir, lower madison river, mt. *Climatic Change*, 68(3):331–353.

489 Gower, J. C. (1966). Some distance properties of latent root and vector methods  
490 used in multivariate analysis. *Biometrika*, 53(3/4):325–338.

491 Harvey, A. C. (1990). *Forecasting, structural time series models and the Kalman*  
492 *filter*. Cambridge university press.

493 Hill, R. A., Weber, M. H., Leibowitz, S. G., Olsen, A. R., and Thornbrugh, D. J.  
494 (2016). The stream-catchment (streamcat) dataset: A database of watershed  
495 metrics for the conterminous united states. *JAWRA Journal of the American*  
496 *Water Resources Association*, 52(1):120–128.

497 Holmes, E. E., Ward, E. J., and Wills, K. (2012). Marss: Multivariate autore-  
498 gressive state-space models for analyzing time-series data. *The R Journal*,  
499 4(1):11–19.

500 Kristensen, K., Nielsen, A., Berg, C. W., Skaug, H., and Bell, B. (2015).  
501 Tmb: automatic differentiation and laplace approximation. *arXiv preprint*  
502 *arXiv:1509.00660*.

503 Kristensen, K., Nielsen, A., Berg, C. W., Skaug, H., and Bell, B. M. (2016).  
504 TMB: Automatic differentiation and Laplace approximation. *Journal of Sta-*  
505 *tistical Software*, 70(5):1–21.

506 Lisi, P. J., Schindler, D. E., Bentley, K. T., and Pess, G. R. (2013). Association  
507 between geomorphic attributes of watersheds, water temperature, and salmon  
508 spawn timing in alaskan streams. *Geomorphology*, 185:78–86.

509 Lisi, P. J., Schindler, D. E., Cline, T. J., Scheuerell, M. D., and Walsh, P. B.  
510 (2015). Watershed geomorphology and snowmelt control stream thermal sen-  
511 sitivity to air temperature. *Geophysical Research Letters*, 42(9):3380–3388.

512 Mauger, G., Casola, J., Morgan, H., Strauch, R., Jones, B., Curry, B., Isak-  
513 sen Busch, T., et al. (2015). State of knowledge: Climate change in puget  
514 sound.

515 McCullough, D. A. (1999). *A review and synthesis of effects of alterations to the*  
516 *water temperature regime on freshwater life stages of salmonids, with special*  
517 *reference to Chinook salmon*. US Environmental Protection Agency, Region  
518 10.

519 McKay, L., Bondelid, T., Dewald, T., Johnston, J., Moore, R., and Rea, A.  
520 (2012). Nhdplus version 2: user guide. *National Operational Hydrologic Re-*  
521  *mote Sensing Center, Washington, DC*.

522 Mote, P. W. and Salathe, E. P. (2010). Future climate in the pacific northwest.  
523 *Climatic Change*, 102(1-2):29–50.

524 NOAA (2017). National centers for environmental information, climate at a  
525 glance: U.s. time series. Data retrieved from: [http://www.ncdc.noaa.gov/](http://www.ncdc.noaa.gov/cag/)  
526 [cag/](http://www.ncdc.noaa.gov/cag/) on 11/10/2016.

Olden, J. D. and Naiman, R. J. (2010). Incorporating thermal regimes into environmental flows assessments: modifying dam operations to restore freshwater ecosystem integrity. *Freshwater Biology*, 55(1):86–107.

Poole, G. C. and Berman, C. H. (2001). An ecological perspective on in-stream temperature: natural heat dynamics and mechanisms of human-caused thermal degradation. *Environmental management*, 27(6):787–802.

R Core Team (2017). *R: A Language and Environment for Statistical Computing*. R Foundation for Statistical Computing, Vienna, Austria.

Radeloff, V. C., Nelson, E., Plantinga, A. J., Lewis, D. J., Helmers, D., Lawler, J., Withey, J., Beaudry, F., Martinuzzi, S., Butsic, V., et al. (2012). Economic-based projections of future land use in the conterminous united states under alternative policy scenarios. *Ecological Applications*, 22(3):1036–1049.

Reidy Liermann, C., Olden, J. D., Beechie, T., Kennard, M. J., Skidmore, P., Konrad, C., and Imaki, H. (2012). Hydrogeomorphic classification of washington state rivers to support emerging environmental flow management strategies. *River Research and Applications*, 28(9):1340–1358.

Stanford, J. A. and Ward, J. (2001). Revisiting the serial discontinuity concept. *River Research and Applications*, 17(4-5):303–310.

USDA (2017). National resources conservation service. Data retrieved from: [https://www.nrcs.usda.gov/wps/portal/nrcs/detail/or/snow/?cid=nrcs142p2\\_046350](https://www.nrcs.usda.gov/wps/portal/nrcs/detail/or/snow/?cid=nrcs142p2_046350) on 1/23/2017.

USGS (2017). National water information system. Data retrieved from: [http://www.ecy.wa.gov/programs/eap/fw\\_riv/index.html](http://www.ecy.wa.gov/programs/eap/fw_riv/index.html) on 1/30/2017.

van Vliet, M. T., Franssen, W. H., Yearsley, J. R., Ludwig, F., Haddeland, I., Lettenmaier, D. P., and Kabat, P. (2013). Global river discharge and water temperature under climate change. *Global Environmental Change*, 23(2):450–464.

Von Prause, M. (2017). River and stream water quality monitoring program. Data retrieved from Washington Department of Ecology: [http://www.ecy.wa.gov/programs/eap/fw\\_riv/index.html](http://www.ecy.wa.gov/programs/eap/fw_riv/index.html) on 7/1/2016.

Ward, E. (2017). nwfsc-timeseries/statss: Initial release for time series class.

Ward, J. (1985). Thermal characteristics of running waters. In *Perspectives in Southern Hemisphere Limnology*, pages 31–46. Springer.

Webb, B. and Walling, D. (1997). Complex summer water temperature behaviour below a uk regulating reservoir. *Regulated rivers: research & management*, 13(5):463–477.

- 564 Zuur, A., Tuck, I., and Bailey, N. (2003a). Dynamic factor analysis to estimate  
565 common trends in fisheries time series. *Canadian journal of fisheries and*  
566 *aquatic sciences*, 60(5):542–552.
- 567 Zuur, A. F., Fryer, R., Jolliffe, I., Dekker, R., and Beukema, J. (2003b). Estimat-  
568 ing common trends in multivariate time series using dynamic factor analysis.  
569 *Environmetrics*, 14(7):665–685.

## Appendix A

### Temperature DFA output and diagnostics

The process of selecting the best  $T_{\text{water}}$  and discharge models involved four climate covariates (air temperature, precipitation, snowmelt, and hydrological drought), between 1 and 15 shared trends, four within-and-among-site error structures (see methods), and two expressions of unknown seasonal variation (fixed monthly factors and Fourier series). The most parsimonious models were selected using the Akaike Information Criterion (AIC) in tandem with  $R^2$  (required increase of 1% for each additional parameter), and in each case included air temperature, precipitation, and snowmelt as covariates. The  $T_{\text{water}}$  model also included five shared trends and an independent and unequally distributed error structure among rivers (i.e. diagonal and unequal variance-covariance matrix). The discharge model (not shown) included six trends. All subsequent plots relate to the  $T_{\text{water}}$  model, and alphabetic names correspond to sampling sites (Fig 1).

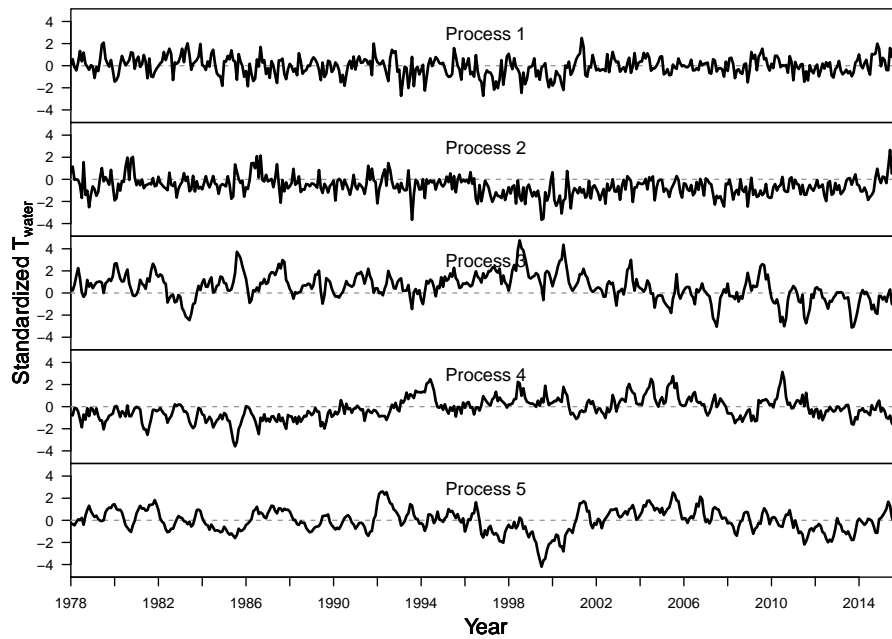
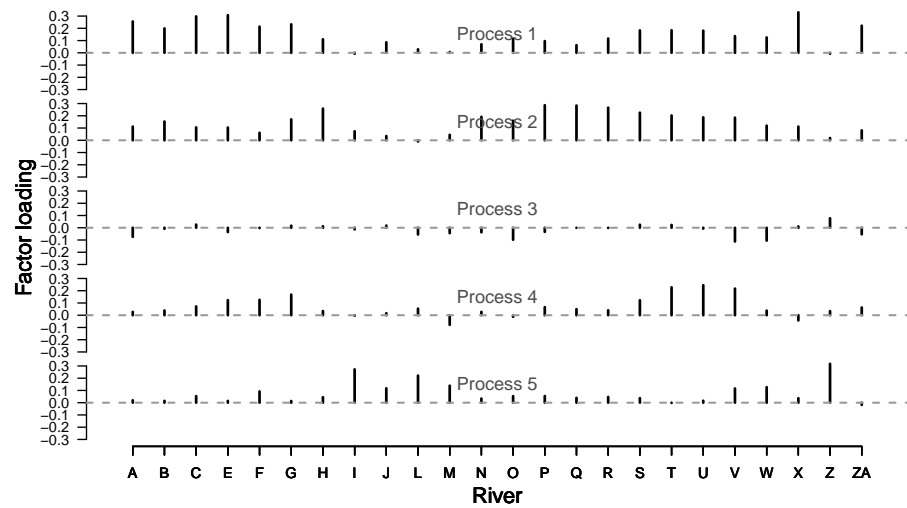


**Figure A1** Shared trends.

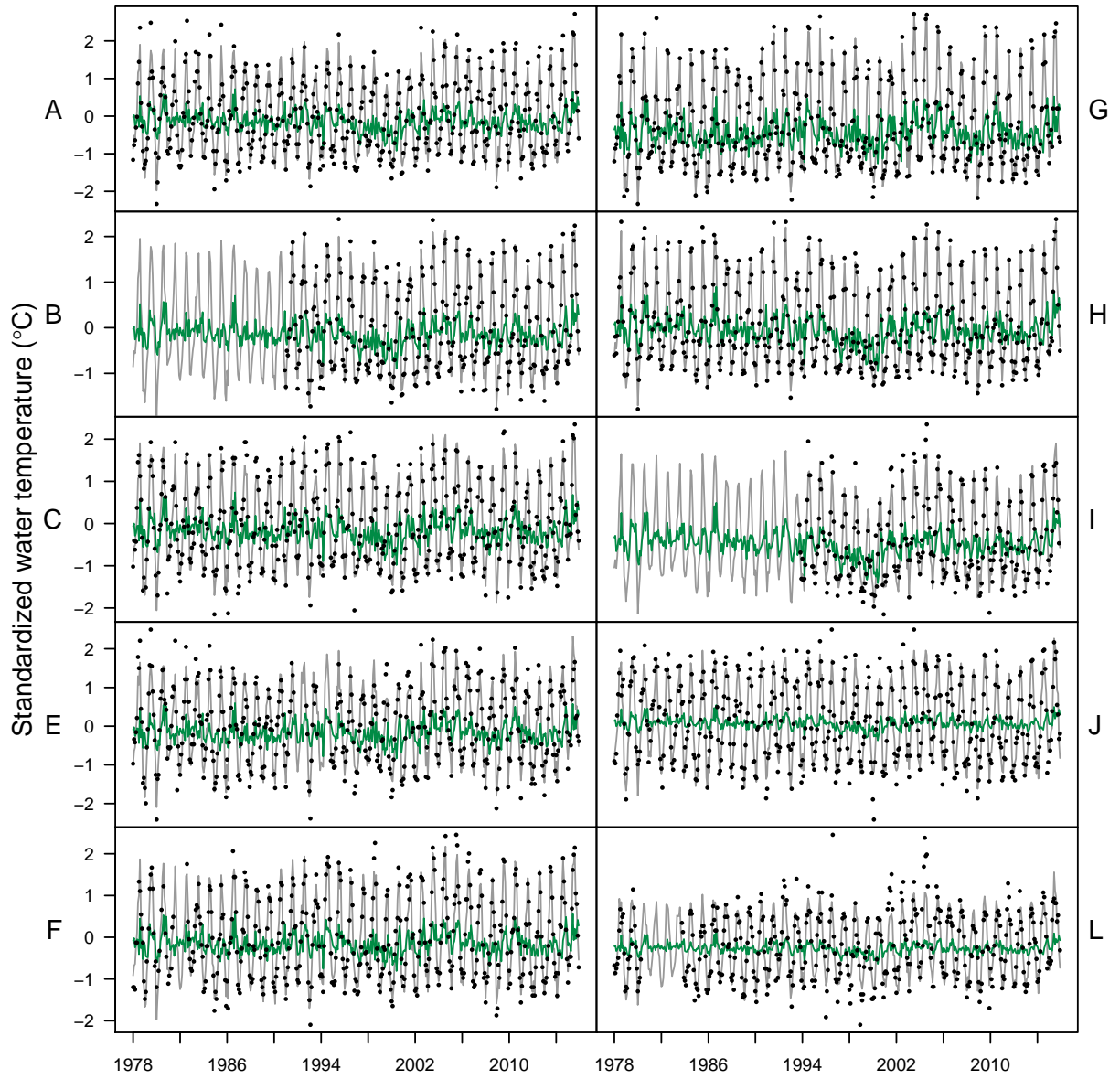


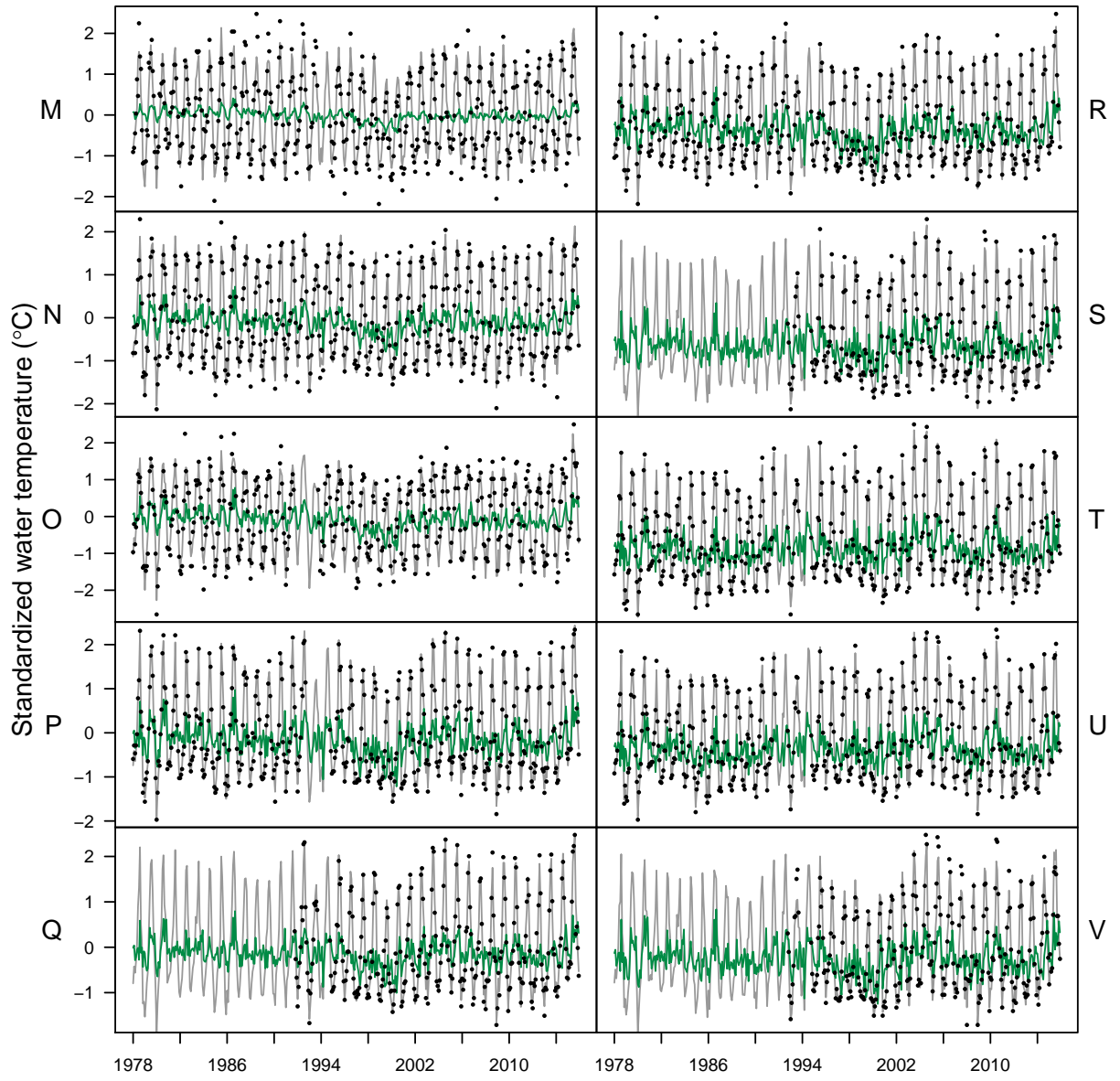
589

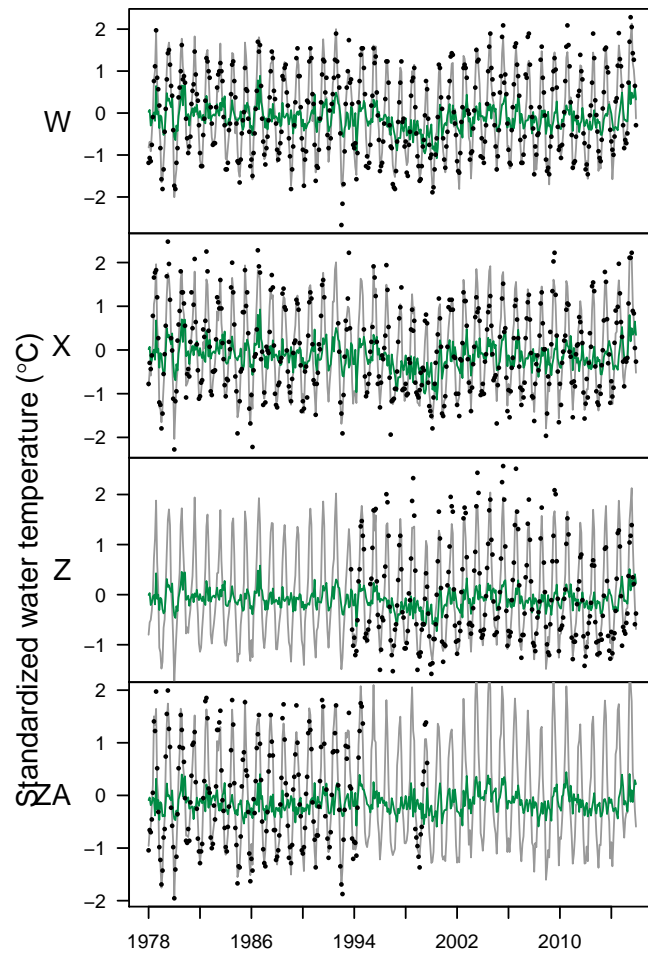
590 **Figure A2** Factor loadings on shared trends.

591



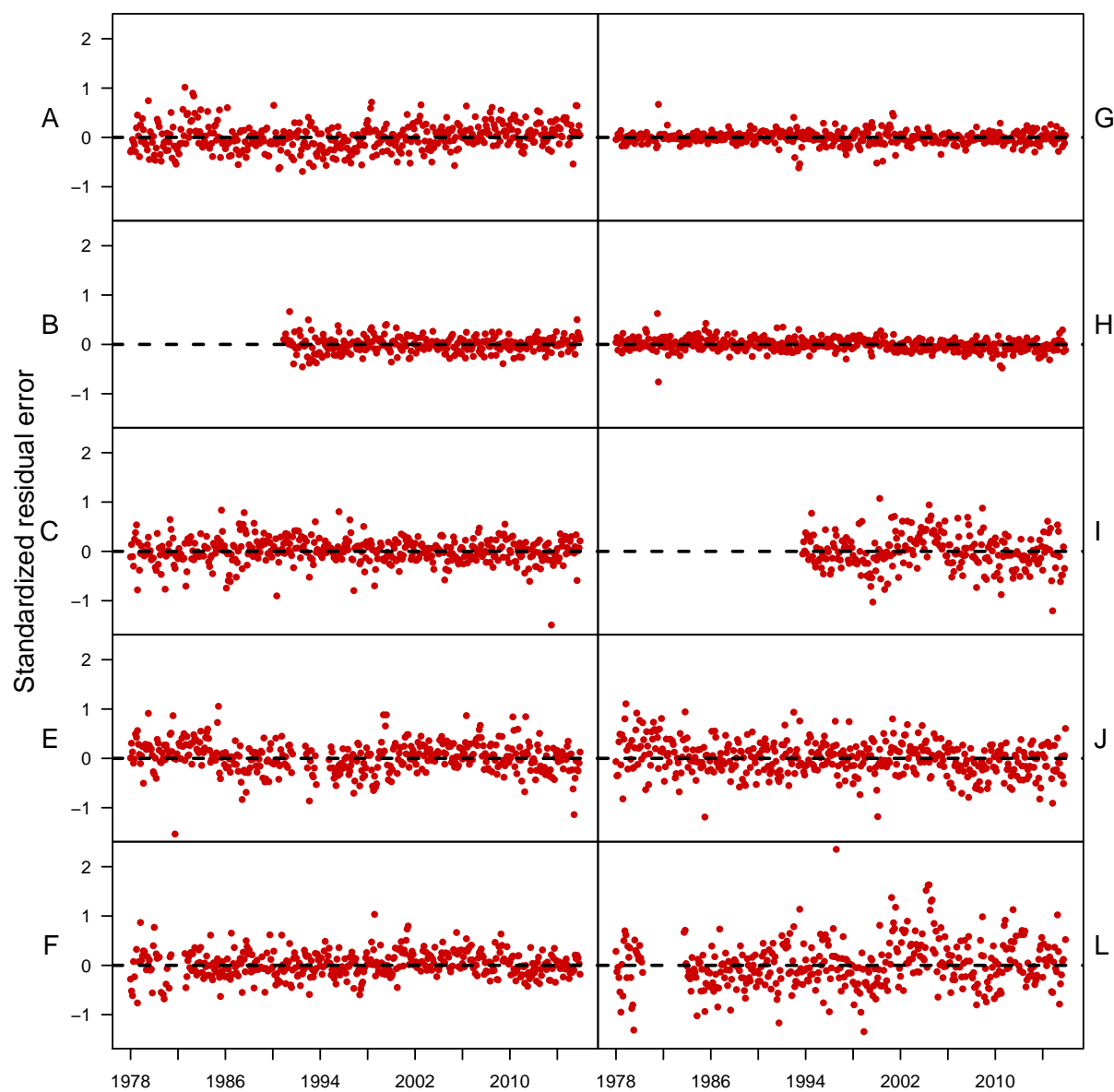


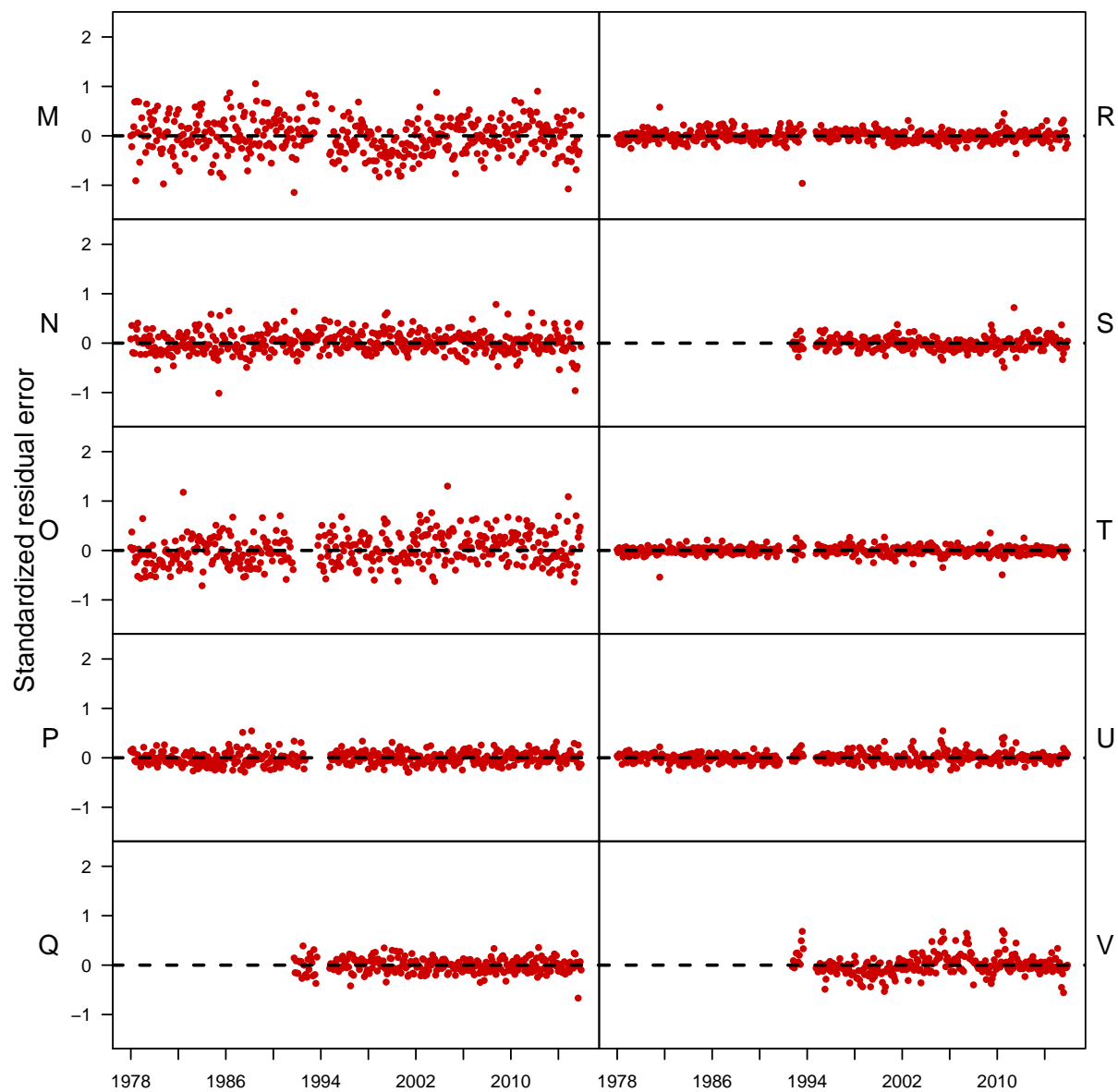


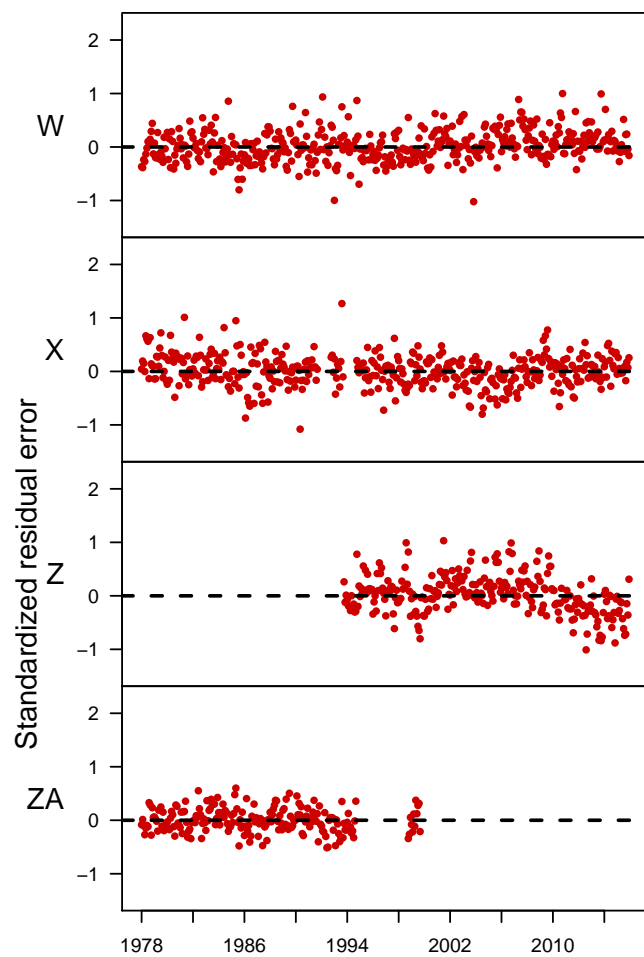


595 **Figure A3** Model fits (gray line = overall fit; green line = trends-only fit, points  
596 = data).

597



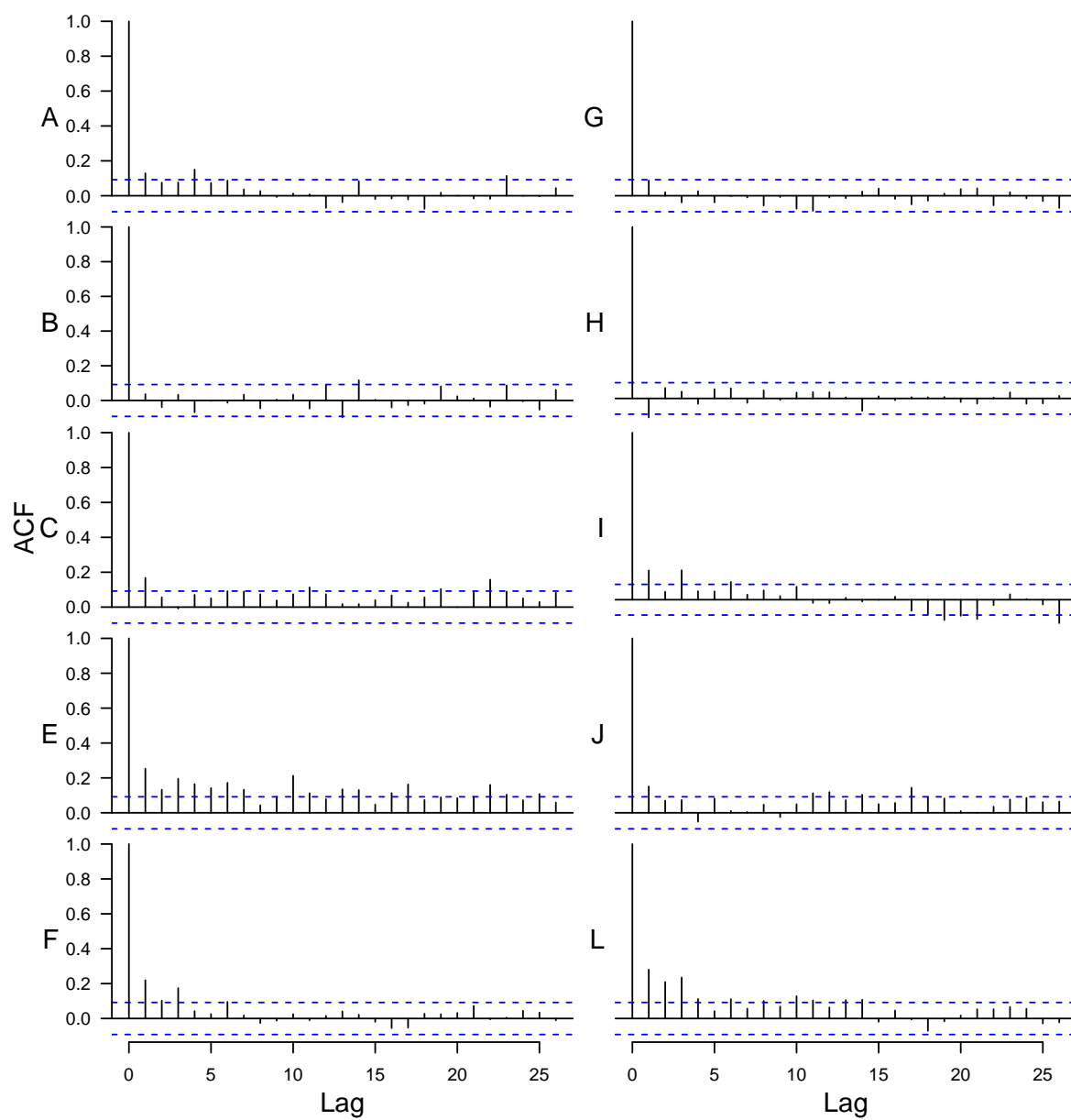


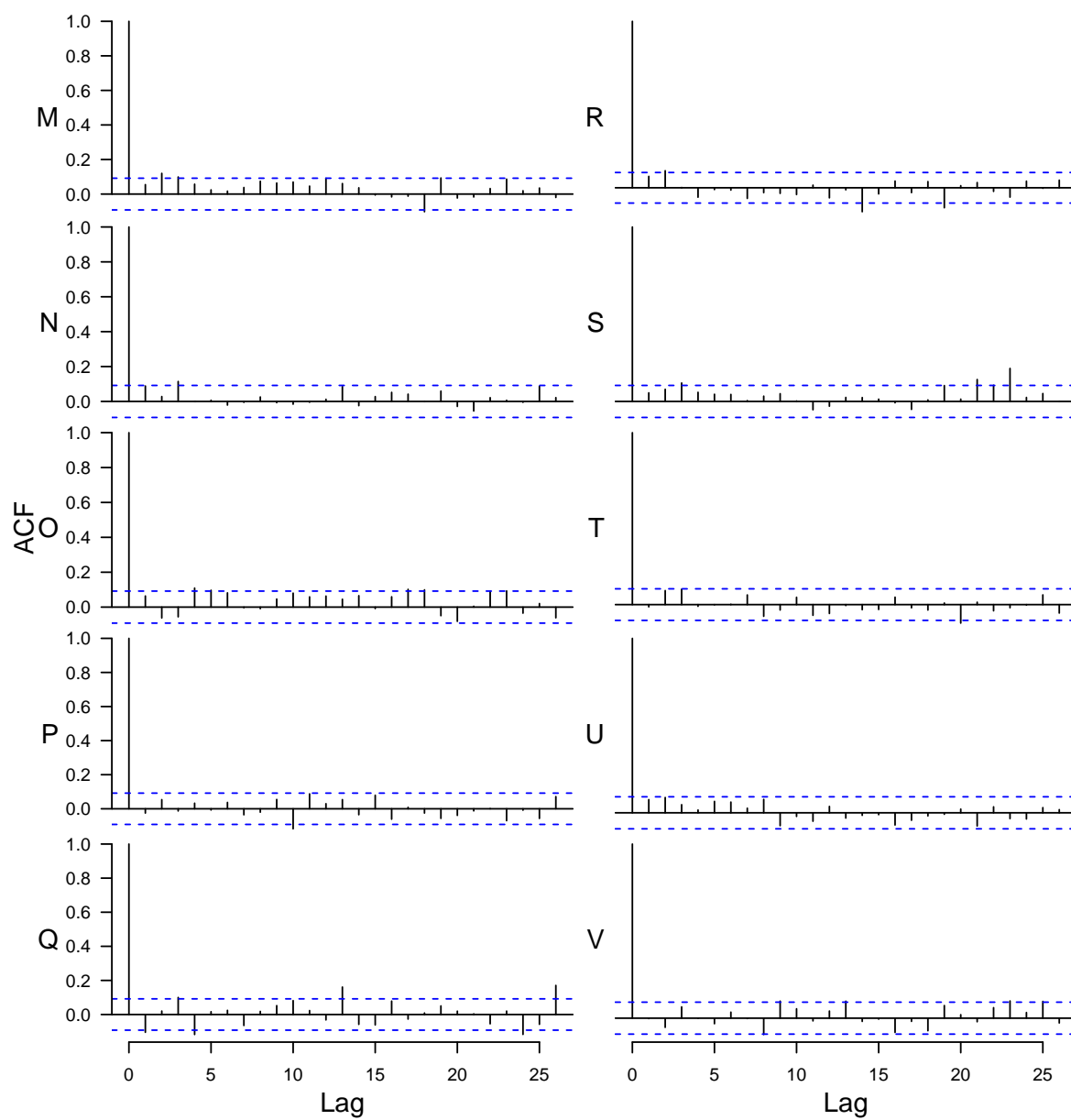


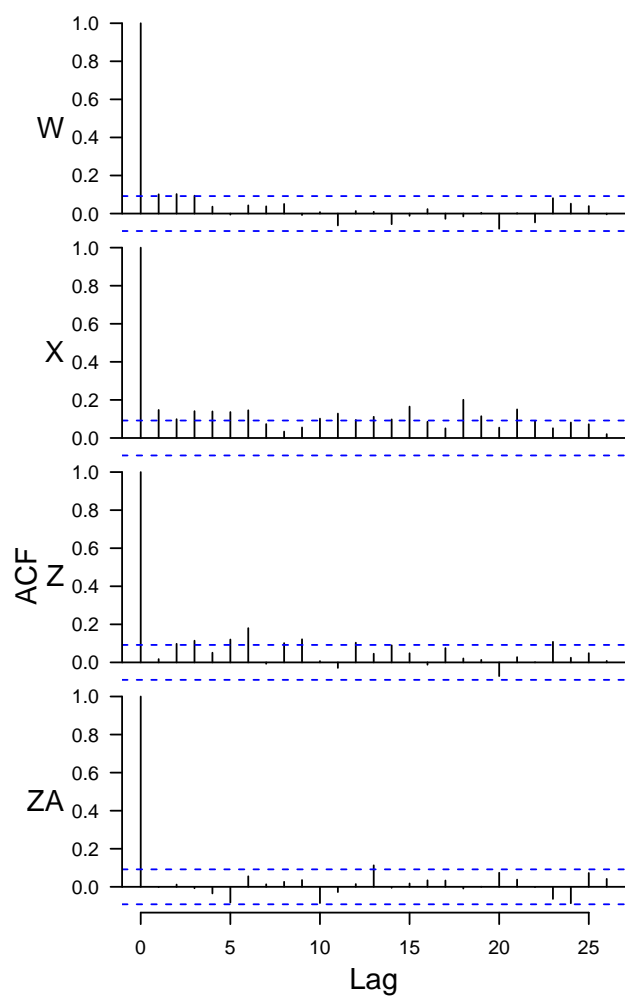
601 **Figure A4** Residuals.

602



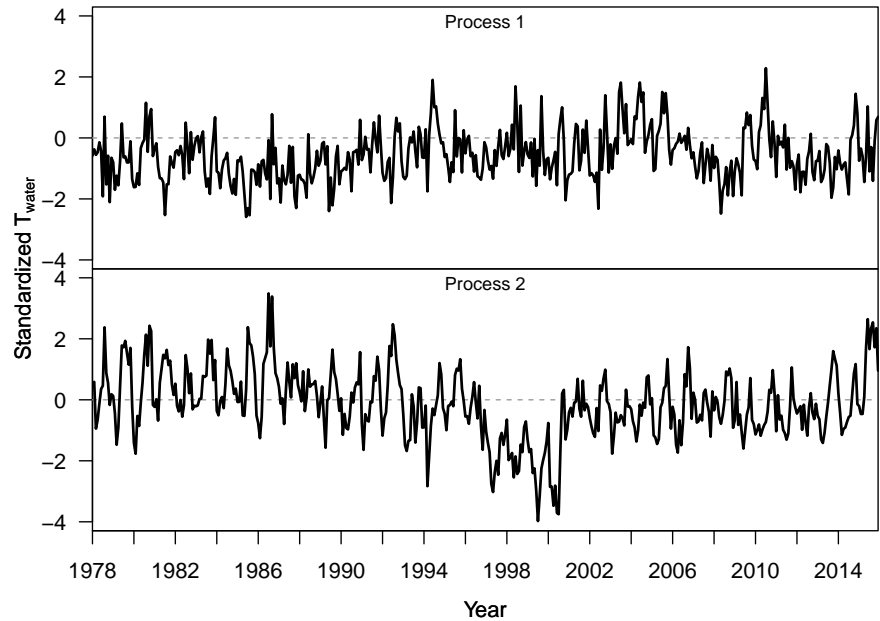






606 **Figure A5** Autocovariance function (ACF).

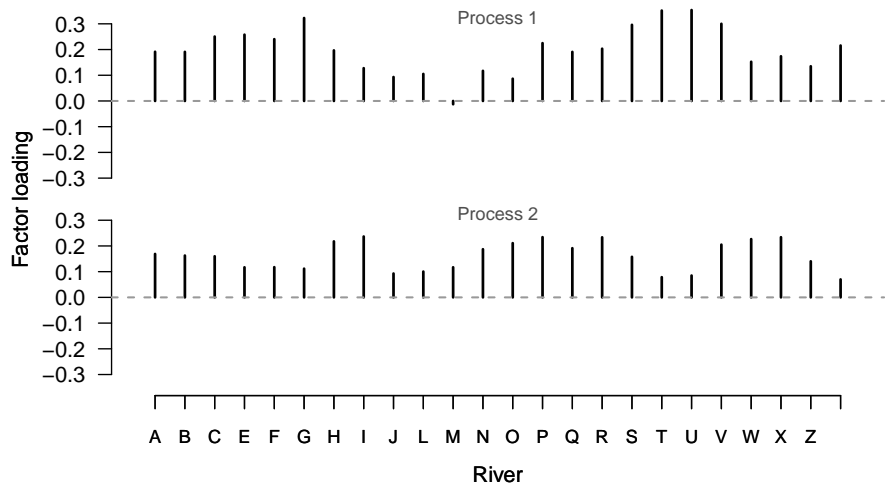
607



608

609 **Figure A6** Shared trends from simplified model (no seasonal fixed factor, no  
610 snowmelt predictor)

611



612

613 **Figure A7** Factor loadings from simplified model (no seasonal fixed factor, no  
614 snowmelt predictor)

## Appendix B

### Testing for change in coupling over time

We used an additional DFA model to test for changes in  $T_{air} \rightarrow T_{water}$  coupling over time, by dividing the 1978-2015 time series into 5 intervals and comparing central tendency and variance of effect sizes for each interval. Figures B1-B3 show mean effect size for each river.

To approximate estimates of variability over time, we performed the same analysis within a Bayesian framework, and obtained uncertainty estimates from the credible intervals of the effect size posteriors. This approach yielded no trends in variation over time, and is not visualized here. For Bayesian analyses, we used R package “statss” (Ward, 2017).

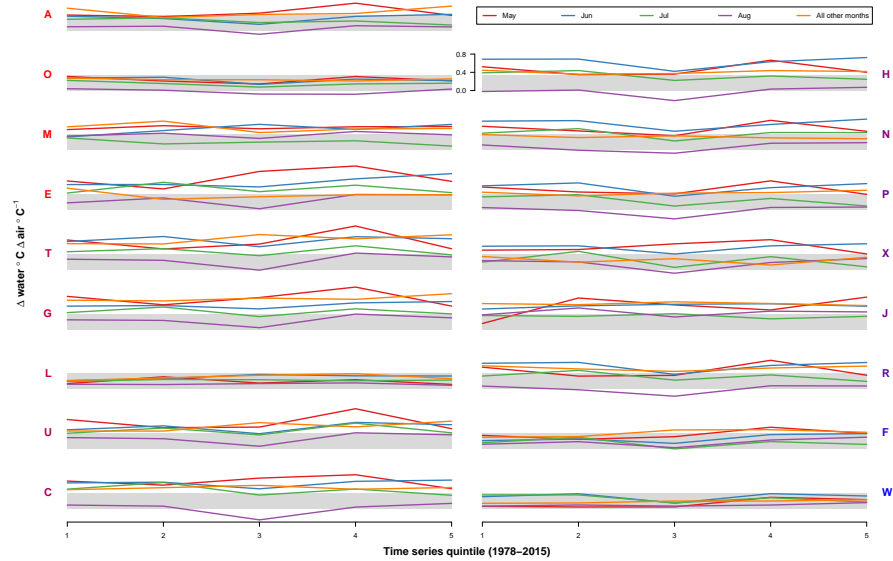


**Figure B1** Mean  $T_{air} \rightarrow T_{water}$  coupling over time. Each plot corresponds to an individual site. Y-label colors represent mean watershed elevation (bluer=higher).

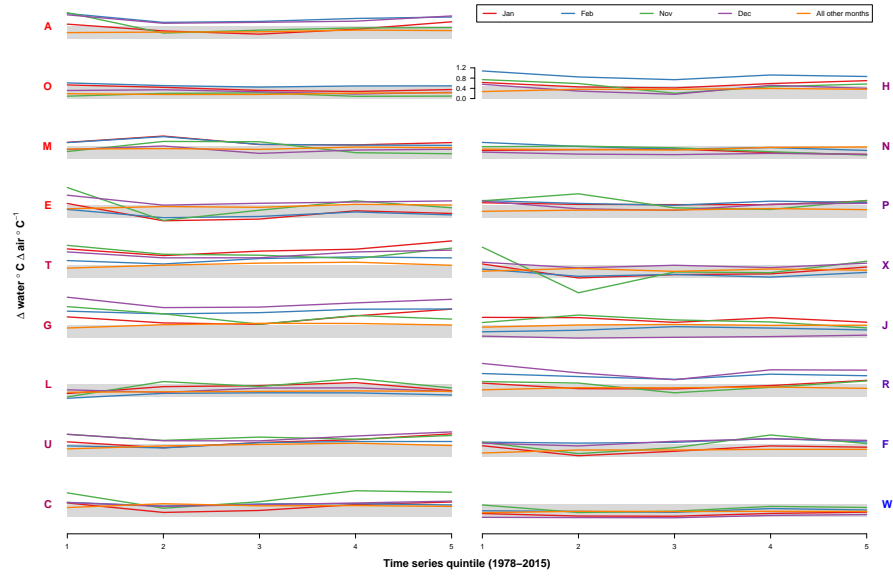


**Figure B2** Mean  $T_{air} \rightarrow T_{water}$  coupling over time. Each plot corresponds to an individual site. Y-label colors represent mean watershed elevation (bluer=higher).



**Figure B3** Mean  $T_{air} \rightarrow T_{water}$  coupling over time. Each plot corresponds to an individual site. Y-label colors represent mean watershed elevation (bluer=higher).

<sup>638</sup> **Appendix C**

<sup>639</sup> **Table C1.**

Site code	DoE ID	Description	Lat.	Long.	Site elev.	Elev.	Area	Area over 1000 m	Slope	Dammed
A	08C070	Cedar R @ Logan St/Renton	47.5	-122.2	4.6	611.3	457.1	0.3	18.1	yes
B	09A080	Green R @ Tukwila	47.5	-122.2	1.2	546.2	1115.7	0.6	23.5	yes
C	01A050	Nooksack R @ Brennan	48.8	-122.6	3	674.5	2046.2	0	5	no
E	03B050	Samish R nr Burlington	48.5	-122.3	11.6	268	225.3	0.2	16.7	no
F	03A060	Skagit R nr Mount Vernon	48.4	-122.3	4.3	1128.3	8035.1	0.2	15.4	partial
G	05A070	Stillaguamish R nr Silvana	48.2	-122.2	10.7	604.1	1456.7	0	6.8	no
H	07A090	Snohomish R @ Snohomish	47.9	-122.1	2.4	688.4	4449.9	0.5	19.2	no
I	16C090	Duckabush R nr Brimmon	47.7	-123	91.4	1047.5	178.6	0.2	13.5	no
J	10A070	Puyallup R @ Meridian	47.2	-122.3	9.1	921	2439.4	0.2	14.1	no
L	16A070	Skokomish R nr Potlatch	47.3	-123.2	18.3	608.8	591.7	0.2	17.1	partial
M	13A060	Deschutes R @ E St Bridge	47	-122.9	28.3	288.2	408.5	0.3	15.7	no
N	09A190	Green R @ Kanaskat	47.3	-121.9	236.2	822.2	659.1	0	5.3	yes
O	08C110	Cedar R nr Landsburg	47.4	-121.9	187.8	808.3	310.3	0.8	25.7	yes
P	07D130	Snoqualmie R @ Snoqualmie	47.5	-121.8	121.9	897.8	946.6	0	11.9	no
Q	07D050	Snoqualmie R @ Monroe	47.8	-122	4.6	638.1	1779.7	0.2	22.8	no
R	07C070	Skykomish R @ Monroe	47.9	-122	13.1	904.6	1986.9	0.3	14.5	no
S	05A110	SF Stillaguamish R nr Granite Falls	48.1	-122	88.4	768.7	308.1	0	8.1	no
T	05A090	SF Stillaguamish R @ Arlington	48.2	-122.1	16.8	625.2	657	0.4	15.7	no
U	05B070	NF Stillaguamish R @ Cicero	48.3	-122	33.5	665.5	667.4	0.4	18.3	no
V	05B110	NF Stillaguamish R nr Darrington	48.3	-121.7	132.6	714.2	222.5	0.3	15.6	no
W	04A100	Skagit R @ Marblemount	48.5	-121.4	109.7	1349.2	3601.1	0.4	14.6	yes
X	01A120	Nooksack R @ No Cedarville	48.8	-122.3	42.7	868.2	1542.7	0.2	9.9	no
Z	18B070	Elwha @ Port Angeles	48.1	-123.6	67.1	1088.6	757.1	0.6	27.5	yes
ZA	08B070	Sammamish R @ Bothell	47.8	-122.2	4.6	147.2	559.8	0.4	19.2	no



Site code	Perenn. ice	Runoff	Bedrock dep.	Water tbl. dep.	Soil perm.	Aspect	BFI	Rip. pop. dens.	Imp. surf.	Urb.	Road dens.
A	0.3	1238.8	143	135.1	14.2	290.6	61.3	81.6	2.9	5.5	3.4
B	2.2	1169.4	140.8	134.6	12.3	295.6	61.1	148.8	4.3	8.2	3.9
C	0	1714.2	139.3	127.2	9	269.1	58.4	26.9	1.2	2.2	1.4
E	0.2	1546	143.2	118.4	12	252.7	52.8	29.2	2.4	5.3	1.8
F	0.6	1998.6	133.5	145.3	7.5	260.8	61.3	5.6	0.6	1.2	0.6
G	0	2563.9	139.8	126.9	7.4	261.5	52	19.6	0.9	1.6	1.3
H	0.3	2255.7	137.2	135	10.9	277.8	57.2	38	1.7	3.5	1.9
I	0.1	1993.8	95.7	172.8	4.7	87.4	54.3	1	0.1	0	0.2
J	0.1	1204.2	145.8	144.4	12.2	295.1	61.5	48.2	2.3	4.5	1.7
L	0.1	1900	112.6	143	7.3	139.2	52.3	2.7	0.5	0.3	1.4
M	0.2	1261.1	139.8	157	17.1	317.2	59.4	70.4	2.1	3.5	2.9
N	0	1165	135.5	152.4	7.7	284.9	59.4	5	0.8	0.9	3.1
O	2.5	1239.9	141.1	139.2	10.4	271.3	59	4.3	0.7	0.5	2.6
P	0	2087.7	135.8	153.4	16.5	243	58.3	18.3	1.4	2.5	2
Q	4	2097.9	139.4	136.8	13.8	270.5	58.6	33.1	1.6	3.1	2.6
R	1.8	2605.6	133.1	143.8	9.3	277.5	56.4	11.1	1	2.1	1.1
S	0	2545	134.5	137.1	6.8	276	54.9	9.4	0.7	1.1	1
T	0	2557.2	137.6	129.5	6.9	280.1	52	23.4	1.1	1.9	1.4
U	0.1	2568.8	140.5	127.9	7.2	272.5	53.1	5.2	0.6	1	1
V	0.1	2562.5	138.2	134.1	6.4	254.4	57.4	3.7	0.5	0.7	1.1
W	3	1806.4	132.1	150.4	6.5	253.8	65.3	0.3	0.5	1.1	0.2
X	0	1715.1	136.6	137.1	7.2	257.9	58.7	5.4	0.6	0.8	1.2
Z	4.4	1599.4	118.3	175	7	323.4	60.4	1	0.1	0	0.2
ZA	2.3	1264.4	143.2	124.1	20.6	339.4	64.2	529.7	14.6	29	6.6